Cost of Locomotion of a Dynamic Hexapedal Robot

David Zarrouk[1], Ronald S. Fearing[2]

Abstract— **In this work we analyze the cost of transport of in-plane hexapedal robots. The robots are modeled as a rigid body with six massless legs, each having two compliant degrees of freedom and the contact is modeled using Coulomb's model. We start our analysis by formulating the cost of transport for rigid legged robots as a function of their geometry, friction coefficients, actuation velocities and slope angle and compare it to the results of a dynamic multibody numeric simulation. In the second part, we estimate the cost of transport in the more general case when the legs and surface are compliant. We evaluate the energy consumptions factors, sliding, work against gravity, elastic losses of the legs and the surface, and kinetic energy and compare them to the total energy input of the actuators. This analysis allows us to evaluate the work range of the robots and determine the optimum locomotion paths for improved battery performance.**

I. INTRODUCTION

Miniature insect-like robots can reach remote areas that are otherwise inaccessible to standard wheeled vehicles or human beings, such as collapsed building or caves, for reconnaissance, maintenance or search and rescue. Many research groups invested considerable effort in investigating hexapedal robots, producing numerous designs, some of which are capable of running at more than ten body lengths per second such as Mini-Whegs [14], Dyna-RoACH[10], DASH [1] and iSprawl [12]. The high crawling velocity presents interesting challenges in terms of stability [4], [9], [10], and maneuverability [14] [15], [20], [21].

The range of the robot is determined by the onboard available energy and the cost of transport (COT). Numerous studies focused on the power efficiency of crawling using the SLIP model, [2], [7], [6], [3], [8], [5], for example. These works described the dynamics of real animals, in the sagittal plane, which, unlike most miniature robots, can optimize their locomotion by changing the contact angle and adapting their leg stiffness to surface conditions [19].

The in-plane dynamics, which become more dominant as the sprawl angle increases, were studied by Schmitt and Holmes [17] [18] and Kukillaya and Holmes [12] who modeled a cockroach as a rigid body which has six legs made of two rigid links connected through active torsional springs. Their study was however limited to sticking conditions of the foot, which do not account for energy dissipation due to sliding or elastic losses. The influence of compliant contact (foot and/or surface) and sliding on the mechanics of crawling was investigated by Zarrouk et al. [22][23] who studied the locomotion of worm robots crawling inside tube-like environments. This analysis was limited to a single DOF sliding quasistatic analysis.

In the present work, we determine the amount of energy required for the locomotion W_{input}, or cost of transport (see [16] for review) defined as

$$COT = \frac{W_{input}}{m\, g\, \Delta d} \tag{1}$$

Where m is the mass of the robot, g is the gravity, and Δd is the locomotion distance. We first analyze the friction forces acting on the rigid legs of a robot which allow us to formulate its velocity as a function of the robot parameters, actuation frequency and slope. Second, we analyze the influence of compliance to the cost of transport and determine the amount of energy lost due to the reduction of speed and dissipation of elastic energy in the legs and surface.

We validate our analysis by comparing the analytical results to a dynamic multibody numerical simulation based on realistic parameters of robots [9] [1]. The simulation allows us also to compare the input energy of the robot through the motors to the different mechanical losses.

II. ROBOT MODEL AND SIMULATION

Similarly to our previous work [23], we use the sliding spring leg (SSL) model and limit our analysis to in-plane dynamics. The SSL model takes into account leg deformation due to ground forces and leg to surface sliding.

A. Robot model

We consider a hexapedal robot consisting of a main body and six actuated flexible legs which rotate around the hip (see Figure 1). Similarly to insects, the robot runs with an alternating tripod gait consisting of a left tripod (LT, legs 1,4,5) and a right tripod (RT, legs 2,3,6). A step begins when a tripod contacts the surface and ends when it disengages, marking the beginning of the next step. A cycle is comprised of two successive steps LT and RT.

The robot has rigid body with a mass m and inertia moment I. The center of mass (COM) of the robot is the geometrical center of the body. The legs are massless and compliant. Each leg has two springs, one along its length (k_l.) and the other at the hip joint (k_r) (see Figure 2). The nominal

[1] Department of EECS, UC Berkeley, (zadavid@berkeley.edu)
[2] Department of EECS, UC Berkeley, (Ronf@eecs.berkeley.edu)

step size L_{step} is defined as

$$L_{step} = 2L_0 \cdot \sin\left(\frac{\alpha_{step}}{2}\right) \tag{2}$$

where L_{leg} is the length of the leg and α_{step} is the step angle measured from the touchdown of the legs until disconnecting from the surface, assuming rigid legs. We define the nominal velocity as the velocity of the legs relative to the robot.

$$V_{nom} = 4 f_c \alpha_{step} L_0 \tag{3}$$

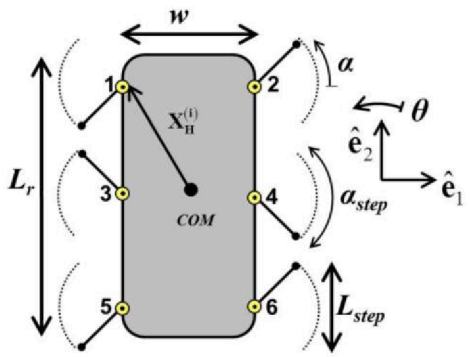

Figure 1 The Hexapod robot model. LT is comprised of legs 1,4,5 and RT is made of legs 2,3,6.

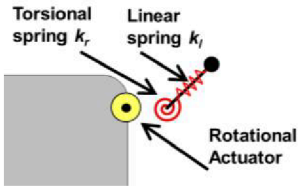

Figure 2. The in-plane model of the legs. Each leg has two elastic DOF, one along its length and a second at the hip.

B. Surface engagement and contact modeling

At the beginning of a step, the robot places its unloaded legs (loose springs) over the surface with no impact and contacts the surface at discrete points at their tip. The leg angle at the beginning of the step is α_0. To model the friction between the robot and surface, we adopt the standard physical model of friction, the Coulomb model. Before sliding, the norm of the friction force is determined by the deformation of the springs. During sliding, the norm of the friction force, $f^{(i,)}$, is the product of the coefficient of friction (COF), μ, and the normal force $F_n^{(i)}$ acting on leg i.

$$\begin{aligned} f^{(i)} &< \mu F_n^{(i)} \qquad \textit{before sliding} \\ f^{(i)} &= \mu F_n^{(i)} \qquad \textit{during sliding} \end{aligned} \tag{4}$$

Since the weight is equally divided between left and right side legs, the norm of the friction force acting on the center leg is roughly double the forces acting on the other legs. Based on the Coulomb friction model, the friction force and the relative velocity of the legs to the surface have the same direction.

C. Dynamic model

The dynamic model is restricted to the horizontal plane. The in-plane forces acting on the robot are the friction forces acting on the tips of the legs and the weight component when running over a slope. As the mass and inertia of the legs are neglected, the forces acting on the hips and on the tips of the legs are identical. The deformations of the linear and torsional springs must satisfy force equilibrium of the tip. The length of the leg is (bold stands for vectors)

$$L^{(i)} = L_0 + \frac{\mathbf{f}^{(i)} \cdot \mathbf{L}_{\mathbf{leg}}^{(i)}}{k_l \mathbf{L}_{\mathbf{leg}}^{(i)}} \tag{5}$$

Vector $\mathbf{L_{leg}}$ is along the length of leg and its norm L_{leg} is the length of the leg. L_0 is the unloaded length of the legs. The load deformation of the torsional spring, due to the moment caused by the friction force, can be calculated using

$$\Delta\alpha_{spring} = \frac{\left|\mathbf{M}^{(i)}\right|}{k_r} = \frac{\left|\mathbf{L}_{\mathbf{leg}}^{(i)} \times \mathbf{f}^{(i)}\right|}{k_r} \tag{6}$$

The forces $\mathbf{f^{(i)}}$ and moments $\mathbf{M^{(i)}}$ act on the robot at the joints of the legs. The dynamic model of the robot is

$$\mathbf{F} = \sum_i \left(\mathbf{f}^{(i)}\right) + \mathbf{F}_{\mathbf{ext}} = m\ddot{\mathbf{X}} \tag{7}$$

where $\mathbf{F_{ext}}$ is an external planar force (weight component for example). The sum of the moments yields the angular acceleration

$$\mathbf{M} = \sum_i \left(\mathbf{X}_{\mathbf{H}}^{(i)} + \mathbf{L}_{\mathbf{leg}}^{(i)}\right) \times \mathbf{F}^{(i)} = I\ddot{\boldsymbol{\theta}} \tag{8}$$

where $\mathbf{X}_{\mathbf{H}}^{(i)}$ is the vector distance between the COM of the robot to the hips of the legs.

D. Numerical simulation

A numerical simulation for the dynamic model of the robot, as per equations (4)-(8), was developed in Matlab based on realistic parameters from existing robot designs [1], [9] and [14]. It is assumed that the angular velocity of the legs is constant and not influenced by the load. Unless otherwise stated, the values of the simulation parameters are m=0.03kg, k_l=100N/m, k_s=100N/m, k_r=0.008Nm, L_0=0.02m, α_0=-π/6rad, α_{step}=π/3 rad, w=0.04m, μ=0.5, the cycle frequency f_c=10Hz, and the slope (defined as the arc tangent of the inclination angle) is λ=0.2. We assume that the kinetic and static COF are the same. Those values are similar to existing centimeter scale robotic designs.

III. ANALYSIS

We start our analysis by assuming rigid legs and contact surface which allow us to formulate the velocity of the legs relative to the surface and determine the direction of the friction forces and total thrust of the robot as a function of the velocity.

A. Friction forces and velocity of the robot

When the legs are rigid, the robot crawls straight with a

velocity V_{robot}. As the legs rotate around the hip of the moving body the instantaneous velocity of the legs is

$$\mathbf{V_{leg}} = \mathbf{V_{robot}} + \dot{\boldsymbol{\alpha}} \times \mathbf{L_{leg}} \tag{9}$$

Where $\mathbf{V_{leg}}$ is the vector velocity of the tips of the legs, $\mathbf{V_{robot}}$ is the velocity of the robot and $\mathbf{L_{leg}}$ is the vector direction of the legs. The velocities of the legs in the directions $\mathbf{e_1}$ and $\mathbf{e_2}$ are respectively V_{leg1} and V_{leg2}

$$\begin{aligned} \left|V_{leg1}\right| &= \left|\dot{\alpha} L_{leg}\, sin\left(\alpha_0 - \dot{\alpha} t\right)\right| \\ V_{leg2} &= V_{Robot} - \dot{\alpha} L_{leg}\, \cos\left(\alpha_0 - \dot{\alpha} t\right) \end{aligned} \tag{10}$$

The sign of V_{leg1} depends on the sign of $\alpha = \alpha_0 - \dot{\alpha} t$ and on whether the leg is on the left or right side of the robot. The thrust of the robot can be expressed as a function of the velocities

$$F_{thrust} = \mu mg \frac{\left|V_{leg2}\right|}{\left(\left(V_{leg1}\right)^2 + \left(V_{leg2}\right)^2\right)^{1/2}} \tag{11}$$

Assuming constant angular speed of the legs and inserting (10) into (11), we obtain

$$F_{Thrust} = \frac{-\mu mg\left(V_{Robot} - \dot{\alpha} L_{leg} \cos\left(\alpha_0 - \dot{\alpha} t\right)\right)}{\left(\left(V_{Robot}\right)^2 + \left(\dot{\alpha} L_{leg}\right)^2 - 2\dot{\alpha} L_{leg} \cos\left(\alpha_0 - \dot{\alpha} t\right) V_{Robot}\right)^{1/2}} \tag{12}$$

Using Newton's second law, the following ordinary differential equation (ODE), whose solution yields the velocity of the robot as a function of time is obtained

$$\dot{V}_{Robot} = \frac{F_{Thrust}\left(V_{robot}\right) + F_{ext}}{m} \tag{13}$$

IV. COST OF TRANSPORT FOR RIGID CONTACT

The cost of transport can be calculated directly from the energy consumption of the motors, by integrating their torque over their angular rotation, or by calculating the different mechanical works such as sliding, work against gravity and change of kinetic energy during acceleration or deceleration, and summing them up. The latter option allows us to compare the contribution of the different works to each other's and to the total energy consumption.

A. Energy input

The battery input energy is transformed into mechanical work through the motors and conveyed to the legs through transmission gears.

$$E_{input} = \frac{W_{locomotion}}{\eta_{mech} \cdot \eta_{electric}} \tag{14}$$

where η_{mech} is the mechanical efficiency of the transmission and $\eta_{electric}$ is the electric efficiency of the motors. Our main interest in this work is in the mechanical energy requirement of the locomotion, therefore we shall disregard the electrical and mechanical losses of the transmission by assuming that η_{mech}=$\eta_{electric}$=1. The work input can be calculated by integrating the torque of the motors over the rotation angle.

$$W_{input} = \sum_i \int_{\alpha_0}^{\alpha_0+\alpha_s} T^{(i)} d\alpha^{(i)} \tag{15}$$

Where the torque $T^{(i)}$, acting on leg i (i is the leg index), is

$$\mathbf{T^{(i)}} = \mu F_n^{(i)} \frac{\mathbf{V_{leg}^{(i)}} \times \mathbf{L_{leg}^{(i)}}}{\left|\mathbf{V_{leg}^{(i)}}\right|\left|\mathbf{L_{leg}^{(i)}}\right|} \tag{16}$$

Figure 3 presents a nearly perfect match between the torque obtained from the Matlab simulation to the torque obtained from the solution of ODE (13) and (16). The torque at the first cycle is substantially higher than in the other ones, as the robot is accelerating and the sliding distance is larger. At the second cycle, the robot reaches steady state. The torque becomes negative shortly after the middle of a step as the legs slide in the same direction of locomotion.

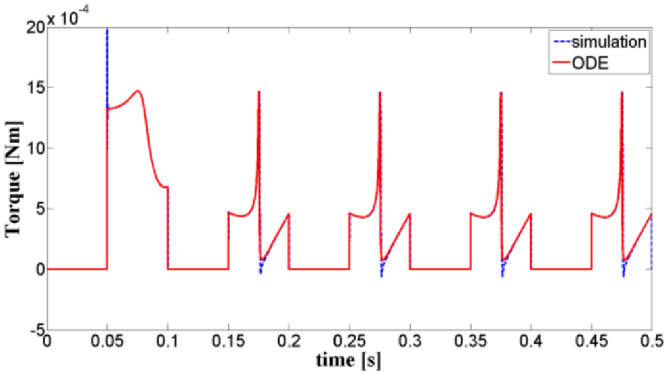

Figure 3. Torque applied by the motor to one of the legs during five cycles.

B. Energy output

When the legs are rigid, the output energy is divided into three categories. Work against gravity, sliding losses, and kinetic energy variation (not losses) during acceleration stages is

$$W_{input} = W_{gravity} + W_{sliding} + \Delta E_k \tag{17}$$

1) Work against a force.

When crawling up a slope, the work required to overcome the weight is

$$W_{gravity} = m\, g \sin\left(\lambda\right) \Delta d \tag{18}$$

where λ is the slope of the surface and Δd is the travelled distance. It should be noted that a resisting force, such as weight, reduces the distance travelled per cycle, up to a complete halt, which results in a substantial increase of other losses such as sliding.

2) Sliding of the rigid legs

The rigid legs will practically slide during the whole step but the direction of the sliding changes as a function of the velocity of the robot and the leg's angular position. The mechanical work done by sliding is

$$W_{sliding} = \mu_k \sum_i \int_t F_n^{(i)} V_{leg}{}^{(i)} dt \qquad (19)$$

Figure 4 illustrates the foot prints of the robot accelerating from rest to a steady state phase. The first footprint is similar to an arc of a circle but its concavity increases with velocity. At full speed, the foot is slower than the robot at touchdown, it goes faster at the middle of the step and slower at the end. The resultant footprint is a gamma like shape.

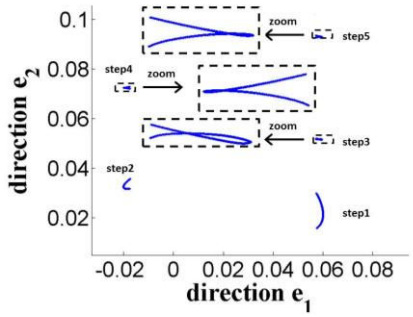

Figure 4. Footprints of the two back legs of the robot crawling. Starting from rest until fifth cycle. Showing the footsteps of legs 5 (left) and 6 (right).

3) Kinetic energy

The kinetic energy of the robot is practically constant during the steady locomotion (which exhibits little velocity changes), but varies during transitions such as the acceleration or deceleration stages. It can be calculated by integrating the net force acting over the robot (thrust force minus gravity forces) over the distance travelled in the specific period.

$$\Delta E_k = \int_x \left(F_{Thrust} - F_{ext} \right) dx \qquad (20)$$

or alternatively, if the velocity is known, it can be calculated as a function of the velocity change

$$\Delta E_k = \frac{1}{2} m \left(\Delta V_{robot} \right)^2 \qquad (21)$$

D. Numerical simulation and comparison to analysis

In this section we use a numerical example based on real robot parameters and calculate the energy as a function of different crawling conditions.

1) Energy requirements starting from rest up to full speed

Figure 5 presents the amount of energy the robot uses as a function of the time. Specifically it compares the energy consumption as a function of the step number starting from rest until reaching steady state speed (roughly 0.4m/s). At the start of run, the robot accelerates and the legs rotate faster than the body, which results in more sliding. The work against gravity increases together with the time and velocity as the robot travels a larger distance. The sum of the kinetic, friction and gravity energies are compared to the energy input of the motor as per equation (15). The comparison shows a nearly perfect match with a maximum numerical error of 0.4%.

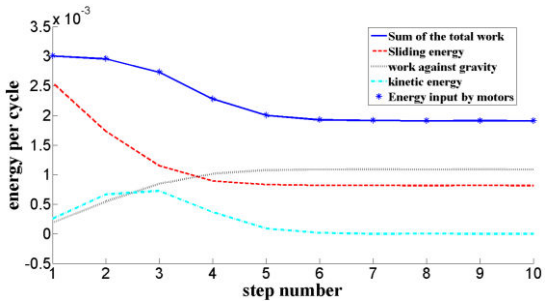

Figure 5 Energy requirements per step starting from rest until steady state velocity.

2) Cost of transport and climbing as a function of the slope.

The cost of transport allows us to determine the amount of energy required per unit distance. Its value increases almost linearly as a function of the slope until reaching a critical angle where the robot cannot advance and the cost of locomotion exponentially increases.

However, in some cases it is important to evaluate the energy required per ascending distance, which we denote by cost of climbing (COC), such as when presented with different paths to the peak of a hill. In this case it is advisable to choose the optimum slope which requires the minimum energy consumption.

$$COC = \frac{W_{input}}{\mathrm{m\,g\,\Delta h}} = \frac{W_{input}}{\mathrm{m\,g\,\Delta d \cdot \sin(\lambda)}} \qquad (22)$$

Figure 6 compares the COT to the COC as function of the slope. The COT and power consumption increases almost linearly until a slope of 0.4 but then the COT increases exponentially as the advance ratio decreases. The optimum slope for minimum COC is 0.3. Changing the slope to 0.2 or 0.4 increases the required consumption by roughly 15 percent. Further change results in an rapid increase as the COC is infinite on a horizontal surface (no climbing at all) or on steep angles (the robot cannot climb the steep slope).

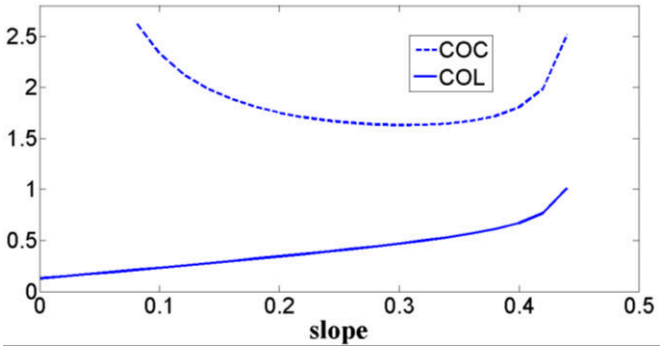

Figure 6. Cost of transport and cost of climbing as a function of the slope. The slope is the arc tangent of the inclination.

V. COMPLIANT LEG ANALYSIS

Flexible legs increase stability and improve grip to rough surfaces but may also increase power consumption by dissipating elastic energy and reducing the net locomotion distance.

A. *Elastic losses of legs and surface*

As the robot detaches its legs from the surface at the end of the step, any elastic energy stored in the legs, is dissipated. The legs model presented as per figure 2 has two compliant DOF, a linear and a torsional. The elastic energy stored in the legs during a step is

$$E_{elastic}^{legs} = \frac{1}{2}\sum_i k_l \left[\Delta l^{(i)}\right]^2 + k_r \left[\Delta\alpha^{(i)}\right]^2 \qquad (23)$$

or alternatively as a function of the friction forces along and perpendicular to the legs

$$E_{elastic}^{legs} = \frac{1}{2}\sum_i \frac{1}{k_L}\left(F_l^{(i)}\right)^2 + \frac{L_{leg}^2}{k_r}\left(F_r^{(i)}\right)^2 \qquad (24)$$

If we assume that the tangential compliance of the surface is linear, such as the case in crawling over grass (Winkler foundation) or Hertzian contact modeling, its elastic energy may be obtained similarly based on the contact force and its compliance k_s

$$E_{elastic}^{surface} = \frac{1}{2}\sum_i \frac{\left(F_l^{(i)}\right)^2 + \left(F_r^{(i)}\right)^2}{k_s} \qquad (25)$$

Combining (25) into (24) we obtain the total elastic energy of the surface and legs as a function of the leg forces

$$E_{elastic}^{total} = \frac{1}{2}\sum_i \left[\left(\frac{1}{k_L}+\frac{1}{k_s}\right)\left(F_l^{(i)}\right)^2 + \left(\frac{L_{leg}^2}{k_r}+\frac{1}{k_s}\right)\left(F_r^{(i)}\right)^2\right] \qquad (26)$$

When all the legs are sliding, the friction force becomes the product of the normal force to the COF and the surface energy simplifies to

$$E_{elastic}^{legs} = \frac{1}{2}\sum_i \frac{\left(\mu F_n^{(i)}\right)^2}{k_s} \qquad (27)$$

And the total elastic energy becomes

$$E_{elastic}^{total} = \frac{1}{2}\sum_i \left[\left(\frac{1}{k_L}\right)\left(F_l^{(i)}\right)^2 + \left(\frac{L_{leg}^2}{k_r}\right)\left(Fr^{(i)}\right)^2 + \frac{\left(\mu F_n^{(i)}\right)^2}{k_s}\right] \qquad (28)$$

Figure 7 presents the change of elastic spring and surface energy during a step. The leg energy increases almost linearly at the loading stage while the elastic surface energy rapidly reaches a constant value at sliding as per equation (27).

B. *Numerical estimate of the different consumption factors*

Using our numerical simulation, we compare the different components of the energy consumption. Figure 8 presents the amount of energy required for the locomotion during a cycle of the robot starting from rest. The elastic energy, calculated as per equation (28), accounts for 15% of the total energy required for the locomotion. The remainder, roughly 85%, is due to sliding and work against gravity. Figure 8 presents the COT as a function of the slope during steady state locomotion. The energy requirement increases linearly as a function of the slope but then exponentially as the robot reaches a critical slope above which it cannot advance. Compared to rigid legs, it is possible to see that the compliant legs COT is slightly lower than rigid legs COT for small slopes but substantially larger for larger slopes.

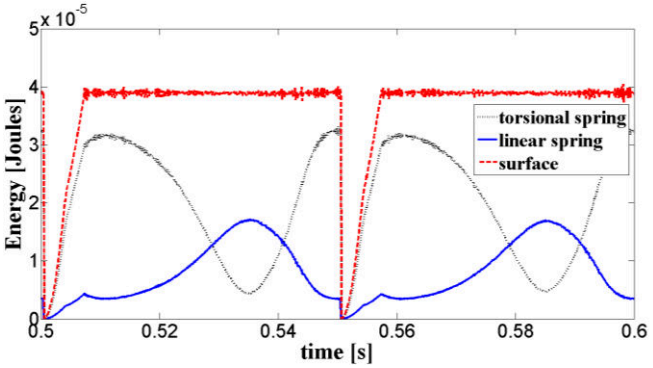

Figure 7. Elastic energy as a function of time.

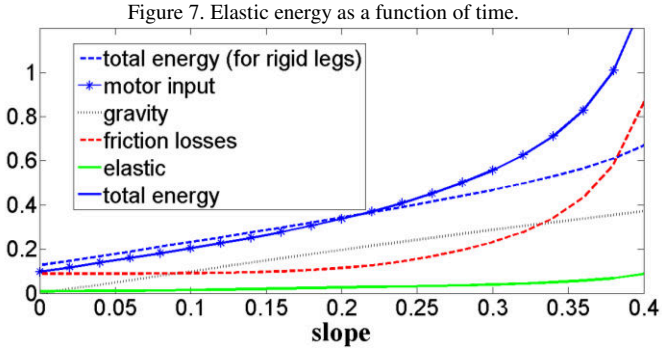

Figure 8. Energy per cycle as a function of an external force as function of the slope. A comparison between the different consumption factors and between the COT for rigid and flexible legs; total flexible legs, total rigid legs and the different losses.

C. *Actuation Frequency*

In steady state, the actuation frequency has a minor effect on the COT as the change of velocity during a step is relatively small. This change becomes even smaller for high actuation frequency as the relative velocity change during a cycle decreases.

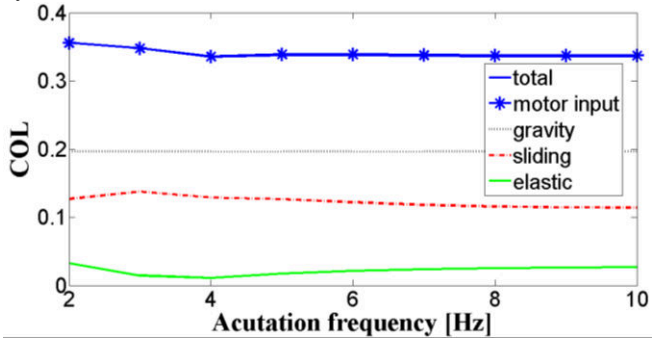

Figure 9. Cost of locomotion as a function of the actuation frequency.

VI. CONCLUSIONS

The research, described in the present manuscript, focuses on the cost of transport of in-plane dynamic hexapedal robot as a function of robot geometry, contact properties, such as compliance, COF, and slope. The results allow an operator to estimate the work range of the robot as well as to be able to choose an optimum path for extended operation time and

distance.

We model the robot as a rigid body with massless but compliant legs and use the Coulomb friction model for the contact model. The influence of environmental properties, such as coefficients of friction, slope and compliance of the surface and their influence to the energy requirements are investigated. A dynamic multibody numerical simulation based on realistic robot parameters was used to compare the different consumption factors.

The friction losses account for most of the energy requirement of the robot and is roughly a linear function of the COF. The elastic energy losses accounted for 10-15% of the losses but the compliance was responsible for a slight increase of the COT as it decreased the velocity of the robot. Interestingly, the COT was found to be practically independent of the actuation frequency of the robot. We defined the COC as the energy required for climbing and derived it as a function of the slope. This result allows an operator to choose an optimum slope for prolonged work range. Finally, the mechanical energy input of the motors was calculated by integrating the torque over the rotation and was compared to the sum of all the outputs (work against gravity, sliding, elastic losses and kinetic energy). The comparison shows a nearly perfect match with maximum relative numerical error of 0.4% (Figure 5).

We anticipate these results to be useful for designing a robot and in decision making algorithms for finding optimum locomotion paths for varying surface conditions. Our future work will focus on determining the influence of leg mass and leg overlapping to the energy consumption.

VII. REFERENCES

[1] P. Birkmeyer, K. Peterson, and R.S. Fearing, "DASH: A dynamic 16g hexapedal robot", IEEE Int. Conf. on Intelligent Robots and Systems, pp. 2683-2689, 2009.

[2] G. A Cavagna, N. C. Heglund, and C. R. Taylor, "Mechanical work in terrestrial locomotion: Two basic mechanisms for minimizing energy expenditure", *American Journal of Physiology,* Vol. 233, No. 5, pp. 243-261, 1977.

[3] M. Carcia, A. Chatterjee, and A. Ruina, "Efficiency, speed, and scaling of two-dimensional passive-dynamic walking", *Dynamics and Stability of Systems: An International Journal*, Vol. 15, No. 2, pp. 75-99, 2000.

[4] R. J. Full, T. Kubow, J. Schmitt, P. Holmes, and D. Koditschek, "Quantifying dynamic stability and maneuverability in legged locomotion", *Integrative and Comparative Biol.* Vol. 42, pp. 149-157, 2002.

[5] R. J. Full, and M. S. Tu, "Mechanics of six legged runners", *Journal of Exp. Biol,*. Vol. 148, pp. 129-146, 1990.

[6] M. Gomes and A. Ruina, "A walking model with no energy cost", *Physical Review E,* Vol. 83, No. 3, 032901, 2011.

[7] N. C. Heglund, M. A. Fedak, C. R. Taylor, and G. A. Cavagna, "Energetics and mechanics of terrestrial locomotion. IV. Total mechanical energy changes as a function of speed and body size in birds and mammals", *Journal of Exp. Biol.*, Vol. 97, pp. 57-66, 1997.

[8] N. C. Heglund, M. A. Fedak, C. R. Taylor and G. A. Cavagna. "Energetics and mechanics of terrestrial locomotion", *Journal of Exp. Biol.*, Vol. 97, pp. 57-66*,* 1982.

[9] P. Holmes, R. J. Full, D. Koditschek, J. Guckenheimer, "The dynamics of legged locomotion: models, analyses and challenges", *SIAM Review*, Vol. 48, No. 2, pp. 207-304.

[10] A. M. Hoover, S. Burden, X.Y. Fu, S. S. Sastry, and R. Fearing, "Bio-inspired design and dynamic maneuverability of a minimally actuated six-legged robot", IEEE International Conference on Biomedical Robotics and Biomechatronics, pp. 869-873, 2010.

[11] D. L. Jindrich, and R. Full, "Dynamic stabilization of rapid hexapedal locomotion", *Journal of Exp. Biol.*, Vol. 205, pp. 2803-2823, 2002.

[12] R. P. Kukillaya, P. Holmes, "A hexapedal jointed-leg model for insect locomotion in the horizontal plane", *Biol. Cyber.*, Vol. 97, No. 5-6, pp. 379-395, 2007.

[13] S. Kim, J. E. Clark, and M. R. Cutkosky, "iSprawl: Design and turning of high-speed autonomous open-loop running", *The Int. Journal of Robotic Research*, Vol. 25, No.9. pp. 903-912, 2006.

[14] J. M. Morrey, B. Lambrecht, A.D. Horchler, R. E. Ritzmann, and R.D. Quinn, "Highly mobile and robust small quadruped robots", IEEE Int. Conf. on Intelligent Robots and Systems, Vol. 1, pp. 82-87, 2003.

[15] A. O. Pullin, N. J. Kohut, D. Zarrouk, and R.S. Fearing, "Dynamic turning of 13cm robot comparing tail and differential drive", IEEE Int. Conf. on Robotics and Automation, pp. 5083-5093, 2012.

[16] A. Ruina, J. E. A. Bertram, M. Srinivasan, "A collisional model of the energetic cost of support work qualitatively explains leg sequencing in walking and galloping, pseudo-elastic leg behavior in running and the walk-to-run transition", *Journal of theoretical Biology*, Vol. 237, pp. 170-192, 2005.

[17] J. Schmitt, P. Holmes, "Mechanical models for insect locomotion: dynamics and stability in the horizontal plane I. Theory", *Biol. Cyber.* Vol. 83, pp. 501-515, 2000.

[18] J. Schmitt, P. Holmes, "Mechanical models for insect locomotion: dynamics and stability in the horizontal plane II. Application", *Biol. Cyber.* Vol. 83, pp. 517-527, 2000.

[19] A. J. Spence, S. Revzen, J. Seipel, C. Mullenes, and R. J. Full, "Insects running on elastic surfaces", *Journal of Exp. Biol.*, Vol. 213, pp. 1907-1920, 2010.

[20] K. Tsujita, H. Toui, and K. Tsuchiya, "Dynamic turning control of a quadruped robot using nonlinear oscillators", Proc. IEEE/RSJ Int. Conf. on Intelligent Robots and Systems, pp. 969-974, 2004.

[21] J. D. Weingarten, G. A. D. Lopes, M. Buehler, R. E. Groff, and D. E. Koditschek, "Automated gait adaptation for legged robots", IEEE Int. Conf. on Robotics and Automation, pp. 2153-2158, 2004.

[22] D. Zarrouk, I. Sharf, and M. Shoham, "Analysis of worm-like robotics locomotion on compliant surfaces", *IEEE, Trans. on Biomedical Engineering*, Vol. 58, No. 2, pp. 301-309, 2011.

[23] D. Zarrouk, I. Sharf, M. Shoham, "Conditions for worm-robot locomotion in flexible environment: Theory and experiments", *IEEE Trans. on Biomedical Eng.*, Vol. 59, No. 4, pp. 1057-1067, 2012.

[24] D. Zarrouk, R.S. Fearing, "Compliance-based dynamic steering for hexapods", IEEE, Int. Conf. on Intelligent Robots and Systems, pp. 3093-3098, 2012.